Provided for non-commercial research and education use.
Not for reproduction, distribution or commercial use.

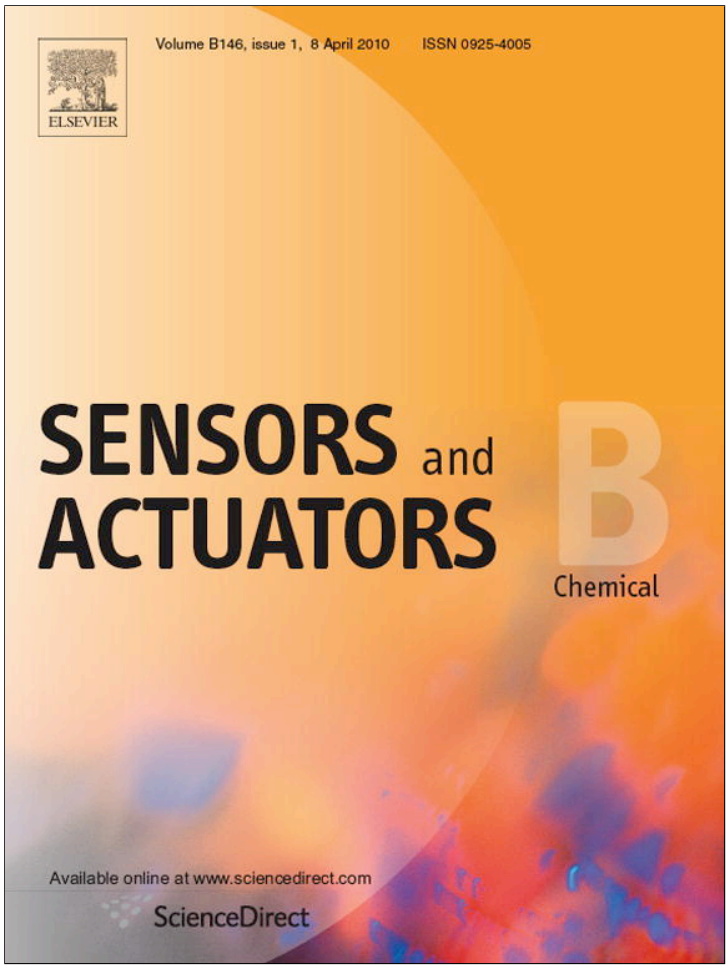

This article appeared in a journal published by Elsevier. The attached copy is furnished to the author for internal non-commercial research and education use, including for instruction at the authors institution and sharing with colleagues.

Other uses, including reproduction and distribution, or selling or licensing copies, or posting to personal, institutional or third party websites are prohibited.

In most cases authors are permitted to post their version of the article (e.g. in Word or Tex form) to their personal website or institutional repository. Authors requiring further information regarding Elsevier's archiving and manuscript policies are encouraged to visit:

http://www.elsevier.com/copyright

Author's personal copy

Sensors and Actuators B 146 (2010) 245–252

Contents lists available at ScienceDirect

Sensors and Actuators B: Chemical

journal homepage: www.elsevier.com/locate/snb

Interferometric readout of multiple cantilever sensors in liquid samples

Stephan T. Koev[a,c], William E. Bentley[b,d], Reza Ghodssi[a,c,*]

[a] Department of Electrical and Computer Engineering, University of Maryland, College Park, MD 20742, USA
[b] Fischell Department of Bioengineering, University of Maryland, College Park, MD 20742, USA
[c] Institute for Systems Research, University of Maryland, College Park, MD 20742, USA
[d] University of Maryland Biotechnology Institute, University of Maryland, College Park, MD 20742, USA

ARTICLE INFO

Article history:
Received 30 November 2009
Received in revised form 3 February 2010
Accepted 10 February 2010
Available online 18 February 2010

Keywords:
Cantilever
Interferometry
Microscope
Array
Homocysteine

ABSTRACT

Microcantilever sensors in the static mode are a promising technology for chemical and biological detection in liquid phase. However, despite their potential for arrayed operation, most demonstrations to date have been performed with single devices due to the limitations of current methods for measuring cantilever displacement. We report a new readout technique using a curved semitransparent SU-8 cantilever on a reflective substrate. The displacement is measured by analyzing the interference pattern in microscope images of the device. Multiple cantilevers are read out with a single microscope by translating the stage to image each device before and after a chemical sample is introduced. Since the images are precisely aligned in software, the position of the stage is not critical, and the image acquisition is rapid. As a proof of principle, the cantilever displacement caused by pH variations or binding of homocysteine is measured. The experiments are performed with 3, 5, or 8 parallel devices exposed either to the same solution or to different sample concentrations. The minimal detectable displacement was determined to be on the order of 1 nm. The presented design and readout method can potentially be adapted for applications such as DNA hybridization assays or immunoassays in array format.

© 2010 Elsevier B.V. All rights reserved.

1. Introduction

Microcantilever sensors have been demonstrated as sensitive tools for chemical and biological detection on chip [1–4]. Their major advantages are small size, label-free detection of the analyte, and potential for arrayed operation. Microcantilevers can be used in two different modes of operation: static and dynamic. In the static mode, the binding of target molecules to the cantilever is detected as a result of the surface stress and cantilever bending they cause [5,6]. In the dynamic mode the cantilever is actuated and its resonant frequency is determined. The binding of the molecules is detected due to the mass change and resulting resonant frequency shift [7,8]. Resonant cantilevers immersed in liquid suffer from high damping losses and reduced sensitivity [1,9]. For this reason, the dynamic mode is normally limited to the detection of gas-phase samples, while the static mode can be used for both gas and liquid samples.

One of the major difficulties of cantilever sensing in either mode is the measurement of cantilever displacement. The most common method for this measurement is the optical lever approach [3,10–14]. A focused laser beam is reflected off the cantilever surface, and captured by a PSD (Position Sensitive Detector). The cantilever displacement causes movement of the laser spot on the PSD and a change in its output voltage. This method is very sensitive, but it requires elaborate free-space optics with precise alignment of the laser beam to the device under test. Moreover, the ratio of PSD signal to cantilever displacement depends on the exact position of the laser spot on the cantilever. This ratio is unimportant for resonant frequency measurements, but it greatly impacts static mode operation. For example, a change in PSD output due to slight laser misalignment can be misinterpreted as cantilever bending. Since the alignment cannot be perfectly reproduced, the laser must be kept aligned to the cantilever throughout the static mode experiment. This precludes parallel measurements. If a cantilever array is exposed to a sample, the response of only one device can be captured. Custom-made arrays of lasers and PSDs for measuring several cantilevers in parallel have been demonstrated [12–14]. However, this approach leads to greatly increased instrumentation complexity and difficulty of alignment. It is not feasible to increase the number of lasers much further, while the number of cantilevers on a chip can easily be in the hundreds or even thousands.

Another common method for measuring cantilever response involves the integration of on-chip displacement sensors. This approach not only allows multiple devices to be measured in parallel, but also simplifies the external measurement setup. The built-in sensors can be piezoresistive [15,16], piezoelectric [17,18], capacitive [19,20], transistor-based [21], or optical [22–24]. Unfor-

* Corresponding author. Tel.: +1 301 405 8158; fax: +1 301 314 9920.
E-mail addresses: skoev@nist.gov, koev@umd.edu (S.T. Koev), bentley@umd.edu (W.E. Bentley), ghodssi@umd.edu (R. Ghodssi).

0925-4005/$ – see front matter © 2010 Elsevier B.V. All rights reserved.
doi:10.1016/j.snb.2010.02.038

Author's personal copy

tunately, all of these technologies greatly increase the fabrication complexity and cost of the cantilevers, which should be simple, cheap and disposable. For cantilever arrays, multiple electrical or optical connections must be made from the sensors to off-chip components, complicating the packaging. Moreover, the resolution of the integrated displacement sensors is typically low due to electrical noise. The output from the sensors is an electrical or optical signal; converting that into actual displacement requires calibration, which may change from device to device. Therefore, comparing the results from multiple cantilevers may be problematic. The integrated sensor readout may be appropriate for applications where portability is essential while the sensitivity, repeatability, and cost are not primary concerns.

This paper presents a new readout technique for measuring static mode displacement that makes use of the intrinsic curvature of SU-8 cantilevers. When the device is imaged with an optical microscope under laser illumination, an interference pattern is formed by light reflected off the cantilever and light reflected off the substrate. The number and position of interference fringes depend on the distance of the cantilever from the substrate; the cantilever's vertical displacement causes a horizontal fringe shift. This fringe shift is extracted from digital images by an automated algorithm and is used to calculate the displacement. The technique is demonstrated by measuring cantilever displacement caused by variations in solution pH or by binding of homocysteine. Although actual samples are detected, the main contribution of this paper is the development of the interferometric readout method and not the demonstration of pH or homocysteine sensors. The cantilevers can ultimately be adapted for a variety of sensing application by using an appropriate biomolecular coating as discussed in Section 5.

It should be noted that other interferometric techniques have been used previously for measuring static cantilever displacement [25–27]. However, these methods use elaborate optical setups; also, the interference cavity is external to the chip since it is formed between the cantilever surface and a reference mirror. This means that the measurement is greatly affected by stage vibrations and changes in the refractive index of the medium. In contrast, the interference cavity in this work is formed between the cantilever and the substrate. Due to its short length and mechanical stability, this on-chip cavity is much more immune to refractive index fluctuations and stage vibrations.

Our approach overcomes most of the limitations of the displacement measurement methods described above. Instead of a custom-made free-space optical setup, it uses a standard optical microscope with a digital camera and a PC. Due to the interferometric nature of the measurement, it is immune to light source intensity fluctuations and mechanical stage drifts. The alignment tolerance of the microscope to the device under test is greatly relaxed. Provided that the cantilever is somewhere in the field of view of the camera, the image can be precisely aligned by a software algorithm. This allows the microscope to be moved from cantilever to cantilever to image an entire array before and after introducing a sample. Therefore, the response of the whole array to the sample can be captured with a single microscope. The fabrication of the interferometric cantilevers is relatively simple, and they require no external connections. No sensor calibration is needed, and the results from different devices can be directly compared (assuming a stable laser wavelength).

The main limitation of our method is its poor temporal resolution due to the slow acquisition of digital images. It is only eligible for static mode detection. In addition, it is better suited for measuring the final cantilever displacement rather than the evolution of displacement over time if a large number of devices are monitored. However, based on the available literature on static mode cantilever sensing, the final displacement value should be sufficient for detection.

2. Design and operation

2.1. Device structure

The interferometric cantilever is made of a 2.2 μm thick SU-8 polymer layer on a Si substrate (Fig. 1a). Its nominal dimensions are 100 μm length and 20 μm width. It is coated with a 15 nm Au layer; due to the small gold thickness, it remains transparent to visible light. The reason for coating with a metal is to enable the thiol coupling chemistries used commonly for functionalizing cantilevers with biomolecules [1,3,4]. The beam curves up due to stress gradient in the materials. Thus, the tip of the cantilever is approximately 1–2 μm above the substrate, depending on the processing conditions. Although out-of-plane curvature is typically undesirable in microfabrication, in this case the curvature is actually needed in order to form an interference pattern. In response to the detection of a sample, the cantilever is expected to move up or down relative to its initial position but still remains some distance above the substrate. For sample delivery, the device is capped with a PDMS layer containing microfluidic channels above each cantilever. This will be described later.

Although cantilever sensors are normally based on Si, SiO_2, or Si_3N_4, there have been several demonstrations of SU-8 cantilevers [9,16]. It was thereby shown that SU-8 is generally a suitable material for this purpose both in terms of stability and surface functionalization. The interferometric readout method reported here only requires a curved transparent beam above a reflective substrate. Therefore, it can readily be implemented with SiO_2 or Si_3N_4 cantilevers that have a stress gradient if polymeric material such as SU-8 is undesirable for a given application.

The smallest gap between the cantilever and the substrate is equal to the thickness of the sacrificial layer used to release the cantilever. In the devices presented here, this gap is only ≈30 nm. It may be possible with some solutions to create local attraction of the two surfaces in the small gap region and therefore cause "parasitic" cantilever bending. This potential problem can be easily rectified by increasing the sacrificial layer thickness to several hundred nanometers. This would not appreciably affect the optical properties of the device.

2.2. Principle of operation

Fig. 1b illustrates the formation of the interference pattern when the cantilever is imaged with a microscope. An incident light beam from the microscope illuminator is partly reflected by the cantilever top and bottom surfaces, producing a beam with intensity I_1. The incident beam also passes through the cantilever and reflects off the substrate, producing a beam with intensity I_2. The phase difference between beams **1** and **2** is given by $\phi = 4\pi dn/\lambda + \phi_o$, where d is the distance between the cantilever and the substrate, λ is the optical wavelength, n is the refractive index, and ϕ_o is a constant. The combined intensity of the reflected beams is given by Eq. (1):

$$I_{refl} = I_1 + I_2 + 2\sqrt{I_1 I_2}\,\cos(\phi) = I_1 + I_2 + 2\sqrt{I_1 I_2}\cos\left(\frac{4\pi dn}{\lambda} + \phi_o\right) \quad (1)$$

Since the cantilever has an upward slope, the distance d increases continuously at points along the cantilever. Therefore, I_{refl} goes through consecutive interference maxima and minima, producing an interference pattern along the cantilever (Fig. 1c).

In order to obtain high interference contrast, the microscope light source must have a narrow spectral linewidth. White light sources would create a continuum of interference patterns, flattening the image intensity. In this work, a solid state laser with nominal

Author's personal copy

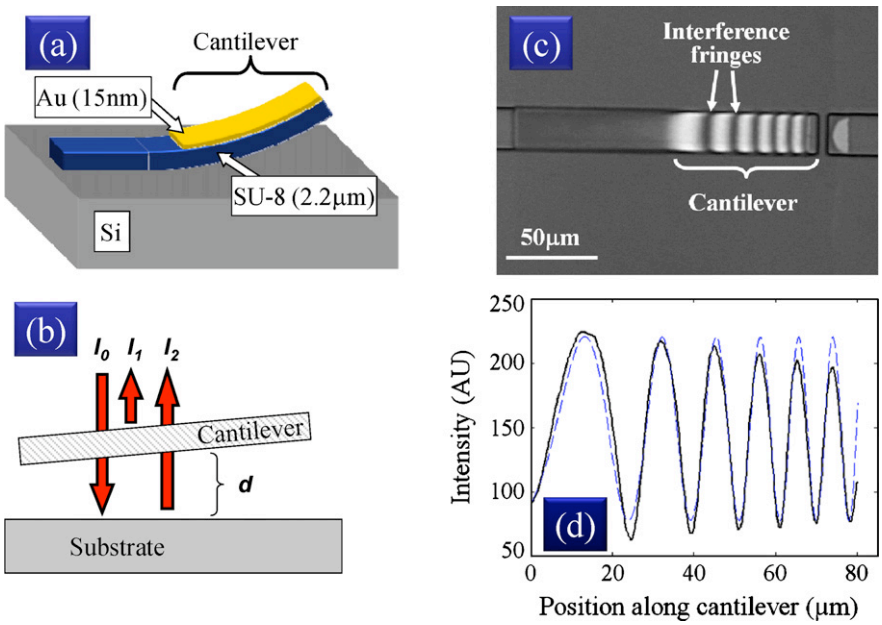

Fig. 1. (a) Schematic of cantilever. (b) Interference between light beams reflected off the cantilever and off the substrate. (c) Microscope image of a fabricated cantilever with a visible interference pattern. (d) Intensity profile measured from cantilever image (solid line) and a least squares curve fit with $R^2 = 0.94$ (dashed line).

wavelength of 660 nm is used as the microscope light source. The laser beam is spatially decohered as described elsewhere [27] to avoid producing a speckle pattern on the image. Sources with somewhat broader spectra, such as LEDs and filtered incandescent light bulbs, also produce visible interference patterns. However, their interference contrast is lower than the one obtained with the laser.

Changes in the interference pattern can be used to find the cantilever vertical displacement upon the detection of a sample. Counting the number of fringes (either minima or maxima) gives a rough estimate of the cantilever tip height. Eq. (1) suggests that each fringe corresponds to an elevation of $\lambda/(2n) = 248$ nm, assuming that $n = 1.33$ (water) and $\lambda = 660$ nm. Large displacements can be estimated by multiplying the change in number of fringes by 248 nm. A more precise determination of the displacement requires a model of the expected cantilever height profile. Cantilevers bent due to residual stress gradient or surface stress should have a parabolic profile of the form $d(x) = a(x - x_o)^2$ [28], where x_o is the position of the cantilever base. Combining this expression with Eq. (1) suggests that the intensity along the cantilever has the form given by Eq. (2).

$$I_{refl}(x) = A + B\cos(Cx^2 + Dx + E) \tag{2}$$

Fig. 1d shows the measured image intensity along a cantilever and a least squares curve fit based on Eq. (2). Overall, the fit agrees well with the measured data ($R^2 = 0.94$), suggesting that the cantilever indeed has a parabolic profile. The intensity envelope of the measured data is affected by the nonuniformity of the microscope illumination, and it deviates considerably from the fit (which assumes uniform illumination). However, the spacing between the interference fringes is determined mainly by the cantilever height profile and is consistent with the fit.

Theoretically, curve fitting can be used for extracting cantilever displacement with much better resolution than the simple fringe counting. However, in practice it has two drawbacks. First, it is difficult to automate because it requires an initial guess. Second, it can introduce appreciable error due to changes in the intensity envelopes of image taken before and after sample detection. We developed another method for measuring small displacements which is more suitable for automation and less sensitive to nonuniform illumination. It is based on measuring the lateral fringe shift that occurs when the cantilever is vertically displaced.

Fig. 2a illustrates a cantilever with an initial height profile C_1 that undergoes displacement into final profile C_2. The horizontal dashed lines represent heights that fulfill the phase conditions for interference fringes. The schematic shows that the downward displacement of the cantilever causes the fringes on the microscope image to move to the right. For example, the fringe of order m moves by Δx. The displacement labeled Δd_1 is given by $\Delta x \cdot \tan(\theta)$. Assuming the cantilever has a parabolic height profile and the height is much smaller than its length (L), the displacement at the tip is given by Eq. (3):

$$\Delta d = \Delta d_1 \frac{L^2}{(L-t)^2} = \Delta x \tan(\theta) \frac{L^2}{(L-t)^2} \approx \Delta x \frac{f_y}{f_x} \frac{L^2}{(L-t)^2} \tag{3}$$

The fringe shift (Δx) and the distance of the fringe from the cantilever tip (t) are measured from the initial and final images of the cantilever by an automated algorithm as described later. The local slope $\tan(\theta)$ cannot be measured directly, but it is approximated by the ratio of the vertical spacing to the horizontal spacing between the fringes on the initial cantilever image, i.e. $\tan(\theta) \approx f_y/f_x$. The error resulting from this approximation will be addressed in Section 4.3. Therefore, the cantilever vertical displacement can be determined based on parameters measured from the microscope images.

2.3. Image registration and fringe shift measurement

To enable rapid measurement of cantilever displacement from the interference images, an automated procedure is necessary for extracting the fringe shift. This is performed by a custom MATLAB program with a graphical user interface. The user selects 2 regions of interest (ROI) with the mouse on each image as shown in Fig. 2b. ROI 1 and 2 contain the fringe whose shift is to be found. An interference minimum is selected here, but a maximum can also be used. ROI 3 contains an adjacent fringe, which serves for finding the fringe spacing and cantilever slope in the initial image. ROI 4 is an alignment feature which enables registration of the images. Although the ROIs are defined manually by the user, the procedure does not require precise selection and takes only a few seconds; the reason

Author's personal copy

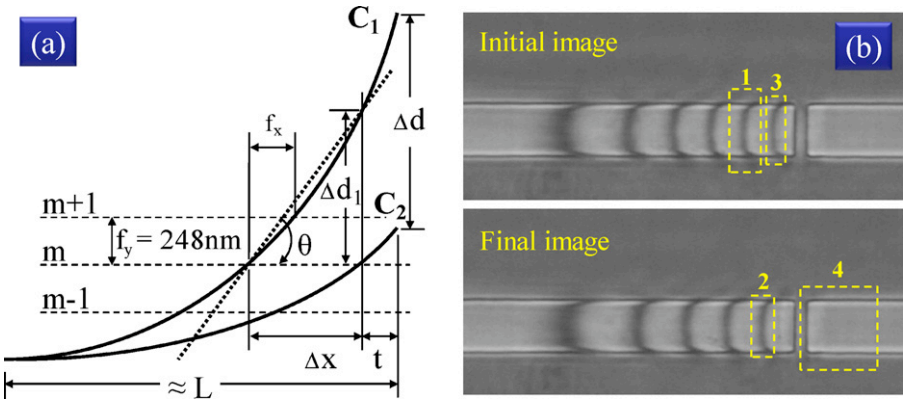

Fig. 2. (a) Geometry used for calculating cantilever displacement from horizontal fringe shift. (b) Initial and final images of a cantilever displaced downward due to change in solution pH. The interference fringes move to the right. The regions of interest 1–4 are selected by the user with the mouse.

for that is that the high-precision measurement is achieved by the algorithm described next.

First, the final image is registered to the initial image since the cantilever may be in a different position within each image due to microscope stage translation. The registration is performed by a well-known method based on the normalized cross-correlation function [29]. Briefly, the coordinates of maximum cross-correlation of ROI 4 (alignment feature) with the initial image are found. This gives the offset that must be applied to the final image to align it with the initial image. The image registration approach is also used for measuring the distance between fringes. The peak cross-correlation between ROI 1 and ROI 2 is found, yielding the fringe shift from initial to final image (Δx). Similarly, the peak cross-correlation between ROI 1 and ROI 3 gives the fringe spacing in the initial image (f_x). Finally, the position of the fringe in ROI 2 is found by a peak-detection function and is used to determine the distance of the fringe from the cantilever tip (t). The described algorithm provides all the parameters needed in Eq. (3) to calculate cantilever displacement.

3. Fabrication and packaging

The fabrication of the cantilevers is described in detail in our earlier work on waveguide-based readout [30]. The devices presented there have a different principle of operation and different layout, but their fabrication process is the same. Control of the cantilever curvature during fabrication is essential. If the curvature is too small, the interference fringes are broad and difficult to locate. If the curvature is too large, the interference fringes are closely spaced and the resolution of displacement measurements is reduced; in addition, the cantilever may extend beyond the depth of focus of the microscope. It was found that curvature between 0.2 mm^{-1} and 0.4 mm^{-1} works well for 100 μm long cantilevers. This corresponds to a height of the cantilever tip above the substrate of 1–2 μm and results in an interference pattern with 4–8 fringes.

The cantilever curvature is caused mainly by two factors: residual stress gradient in the SU-8 and swelling of the SU-8 in liquid. It has been shown that the residual stress gradient is caused by the variation of cross-linking density across the SU-8 thickness, which results from gradients in bake temperature and UV exposure intensity [31]. Therefore, the stress gradient depends on the baking temperature and method (hotplate or oven) and on the exposure dose. Using the SU-8 recipe reported earlier [30], the curvature due to the residual stress gradient was less than 0.1 mm^{-1} for dried cantilevers in air. The remaining contribution to cantilever curvature is due to the swelling of SU-8 when it is immersed in water. The top cantilever surface is covered by metal and does not swell as much as the bottom surface, which is uncoated. This creates a strain gradient and upward beam bending, resulting in a curvature in the range 0.2–0.4 mm^{-1}. As expected, the curvature varies slightly between wafers and between cantilevers on the same wafer due to subtle differences in SU-8 thickness and processing conditions. This has negligible effect on the displacement measurements since each cantilever is referenced to its own initial position.

The water absorption and swelling of SU-8 exhibit a transient response. When a dried cantilever is immersed in water, its curvature increases gradually and reaches equilibrium in several minutes; after that, the cantilever remains stable, and there is no measurable drift. This behavior has also been reported by others. Hill et al. [32] observed that an SU-8 membrane immersed in water drifted at a decreasing rate consistent with a Fickian diffusion model and eventually reached a steady state. Hossenlopp et al. [33] quantitatively studied the water absorption of a 10 μm thick SU-8 film using a quartz resonator and concluded that the film attains equilibrium after approximately 7 min. These results confirm that the SU-8 structures are stable in water if they are given enough time to equilibrate.

The adhesion of SU-8 to the Si substrate in our process was excellent and was not noticeably affected by swelling. No delamination was observed even for devices that were immersed in water for months. Adhesion failure of SU-8 is a commonly reported issue for high aspect ratio structures or large layer thicknesses. The structures used in this work do not fall under either of these categories.

The chips are packaged with a PDMS polymer layer, which defines a separate microfluidic channel over each cantilever (Fig. 2a). The channels are 100 μm deep and 500 μm wide. Prior to packaging, the chips are cleaned by immersion in dilute HCl (concentration 1%, w/w) for 5 min followed by immersion in DI water for 10 min. The PDMS layer is fabricated as described in Ref. [30] and then is aligned on top of the chip while it is kept wet. The PDMS is secured in place with a custom-made clamp that has the appropriate window to allow top-down imaging of the cantilevers with the microscope (Fig. 3b and c). Each channel has an input well as defined by a hole in the PDMS layer and an output capillary connected to Tygon tubing. The sample is placed in the input well with a pipette, and it is sucked into the channel over the cantilever by applying vacuum to the output tubing with a syringe.

4. Measurement results

Two different types of samples were used to demonstrate the measurement of cantilever displacement: dilute hydrochloric acid (HCl) and homocysteine (HC). The samples were dissolved in deionized water (DI) with varying concentrations. First, DI is introduced into the channels; initial images of each cantilever are taken with the microscope by translating the stage. Then, the samples are

Author's personal copy

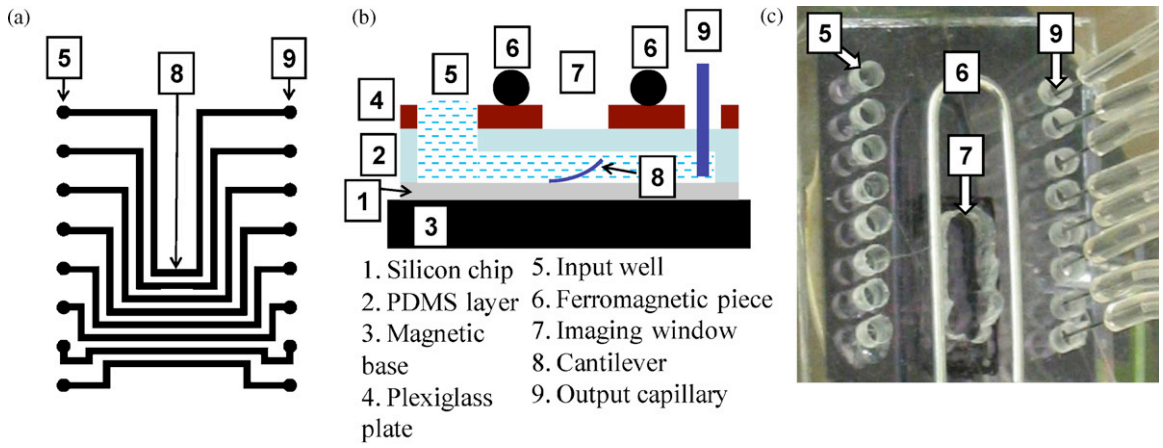

Fig. 3. (a) Layout of fluidic channels. (b) Cross-section schematic of packaged device along a channel. The PDMS is held in place by a clamp consisting of magnetic base, plexiglass cover, and ferromagnetic piece. (c) Top-down photograph of fully packaged chip (width is 2.5 cm).

introduced into the channels. Care is taken to avoid overfilling the input wells and cross-contaminating the samples. Next, images of the displaced cantilevers are taken and saved. Finally, the images are analyzed by the method described in Section 2 to extract the displacement.

All images are acquired at either 20× or 40× optical magnification using a microscope with a manual X-Y stage (Mitutoyo FS70). The camera has 3840 × 3072 pixels (Nikon DXM1200). The resulting image resolution is either 9 or 18 pixels/μm. The microscope's white light source was replaced with a 130 mW diode laser operating at 660 nm (Mitsubishi Electric, Cypress, CA). The laser beam is fed through a spinning diffuser to reduce its spatial coherence and guided into the microscope port with a fiber optic bundle. This custom-made light source is described in detail elsewhere [27].

4.1. Testing with HCl

The gold coated SU-8 cantilever bends down in response to acidic solutions. This effect is probably due to shrinking of the polymer. The bottom of the cantilever is uncoated and shrinks more than the top, which is covered by the metal layer. This pH dependent behavior was used to emulate the cantilever displacement that would occur upon detection of a chemical or biological sample. HCl was dissolved in DI to make solutions with a range of pH values from 0.86 to 4.16. There was a 5 min waiting period between injecting the sample and acquiring the image. The liquid settling time is on the order of several seconds, and the cantilever response time to pH changes was observed to be less than 1 min. The 5 min waiting period ensures that the cantilever has reached equilibrium, although it may be longer than necessary.

Three neighboring cantilevers were imaged in DI and then in samples with decreasing pH. For this experiment, a modified version of the PDMS layer was used such that all cantilevers are in the same fluidic channel. This reduced the number of sample injections needed by a factor of 3. The measured displacements are shown in Fig. 4a (labeled as single-channel experiments). The responses of the 3 devices are quite similar. The observed variations in pH sensitivity are probably due to slight differences in cantilever dimensions and material properties.

Note that one cantilever can be used for detecting multiple consecutive samples if the pH of each sample is lower than that of the previous (as in Fig. 4). However, we observed that if a low pH sample is tested first (i.e. high HCl concentration), the acid absorbed in the SU-8 and PDMS affects the response to subsequent samples with higher pH. In this case, the device can be cleaned and reused by unpackaging it, immersing it in DI water for 10 min, and repackaging it with fresh PDMS.

Next, a chip with 8 cantilevers was tested over the same range of pH values. In this case, each device was in a separate fluidic channel and was exposed to a single sample. In other words, the pH sweep is performed spatially instead of temporally. The measured displacements are shown in Fig. 4a (labeled as multi-channel experiment), and they agree reasonably well with the results from the single-channel test.

The refractive index of HCl is slightly higher than that of DI water, and it may introduce some error in the measurements. The highest refractive index here is that of the highest HCl concentration, which is 0.137 M (pH 0.86). Reported index values of 1.33502 for 0.239 M HCl [34] and 1.33302 for water [34,35] were found in literature. This difference would cause an offset of −3 nm in the displacement measurement (in our convention, downward displacement is positive). Therefore, the error due to the refractive index change is negligible in this case.

If small cantilever displacements or highly concentrated samples are measured, the error can be corrected by taking into account the appropriate refractive indices.

4.2. Testing with homocysteine

The second type of sample detected with the cantilevers is homocysteine. This is an amino acid with a thiol functional group, which has a high binding affinity for gold. Thiol compounds are known to form monolayers on gold surfaces [36] and cre-

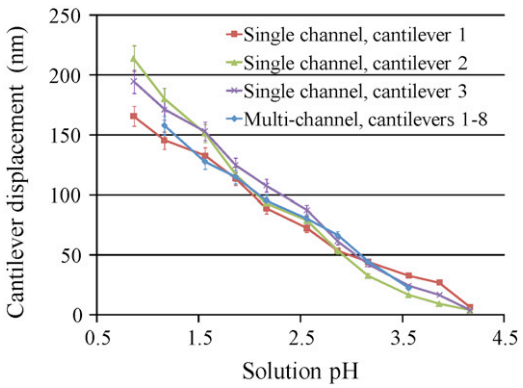

Fig. 4. Measured displacements of cantilevers exposed to samples with different pH. High pH samples injected first followed by low pH samples. Error bars based on measurement error described in Section 4.3.

Author's personal copy

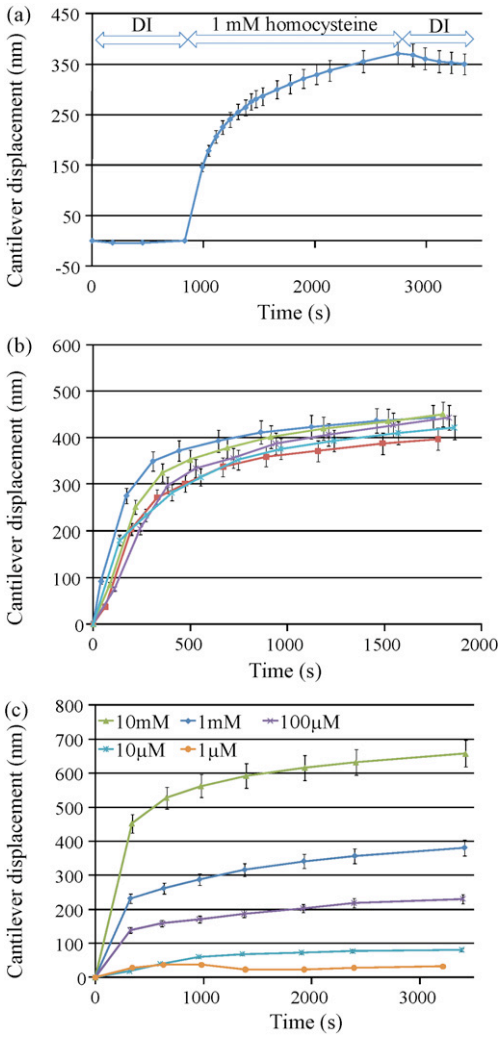

Fig. 5. (a) Response of a single cantilever to 1 mM homocysteine solution. (b) Responses of 5 identical cantilevers to 1 mM homocysteine solution. (c) Responses of 5 identical cantilevers to homocysteine solutions with varying concentrations. (In b and c, the sample is introduced at time 0.) Error bars based on measurement error described in Section 4.3.

ate compressive stress that bends the cantilever down [9,37]. The samples were prepared by dissolving homocysteine powder (Sigma–Aldrich, USA) in DI water.

A single cantilever was tested first to estimate the characteristic timescale of the detection. Fig. 5a shows the measured response to 1 mM solution (the displacement is downward). It has the form of exponential rise to max, which is consistent with the first order kinetics model of the thiol assembly [38]. Approximately 32 min after the sample injection, the sample was flushed and replaced with DI water. Note that there is no abrupt change in displacement at that point, verifying that the difference in refractive index between DI and homocysteine solution is negligible. The displacement decreases gradually after that, probably due to some detachment of homocysteine from the gold surface. The measured max displacement is 370 nm. Using the Stoney equation [39] with our cantilever dimensions and the typical Young's modulus of SU-8 (≈2 GPa) [40], a surface stress of 0.15 N/m due to homocysteine assembly was estimated. This value is within the range 0.08–0.25 N/m, which has been reported in literature for thiol compounds with varying chain lengths [37]. The above conversion of displacement into surface stress is only approximate since the Young's modulus of SU-8 varies considerably with fabrication parameters, and a representative value from literature was used here. For more accurate conversion, the Young's modulus must be tested for the particular process conditions. A variety of techniques have been developed for characterizing the mechanical properties of SU-8 elsewhere [40–42].

Next, 5 cantilevers on a single chip were tested with the same sample concentration (1 mM) as shown in Fig. 5b. The responses are overall very similar, and the variations can be attributed to small differences in cantilever stiffness and gold surface properties. It has been shown that the density of thiol monolayers is greatly affected by defects and contamination of the gold layer [36]. The results presented here are from devices used for detection only once. Larger variations in response were observed when using cantilevers that were cleaned and used for homocysteine detection multiple times (not shown here), presumably due to increasing contamination. The cleaning in these cases was performed by unpackaging the device and immersing it in dilute HCl as described in Section 4.3 for new devices. Although the cleaning did not produce repeatable results, the cantilever is compatible with MEMS batch microfabrication and is extremely low-cost. For this reason, even a single-use, disposable sensor would be acceptable.

Finally, the responses of 5 cantilevers on a single chip were tested, exposing each device to a different homocysteine concentration. There is a clear trend of increasing displacement with concentration (Fig. 5c). This kind of behavior is expected based on the first order kinetics model of thiol assembly [38].

The results demonstrate the ability of our readout method to measure multiple cantilevers in parallel. If this experiment was performed with the conventional PSD method, the reader would have to capture the entire response of one cantilever (∼1 h) before moving to another due to the tight alignment tolerances. Therefore, the total experimental time would be 5 h. Using our method, the responses of all 5 cantilevers are captured in 1 h because the alignment is not critical and the reader can be moved between devices that are simultaneously exposed to samples. Clearly, the ability for parallel measurements would be even more beneficial for larger numbers of cantilevers or longer sample exposure times.

4.3. Measurement error

The error in the interferometric measurements of cantilever displacement can be divided into random and systematic. The random error is due to uncontrollable variations in the measurement setup, such as small changes in microscope focusing and sample positioning, camera noise, and wavelength fluctuations. It was estimated to be less than ±1 nm, leading to a minimal detectable cantilever displacement of 1 nm. The systematic error is mainly due to the slope approximation used in Eq. (3). Its value depends on the exact cantilever profile, and it was estimated to be less that 6% of displacement for the cantilevers used here. The characterization of both types of error is presented in detail as Supplementary Material online.

5. Discussion

The detection of homocysteine and pH changes has little practical significance; it was performed only to demonstrate our device and displacement measurement method. It has already been shown that cantilevers in the static mode are useful tools for biochemical applications. For example, they can detect DNA hybridization [5,6,11,14,26], binding of antigens to antibodies [4,21,43,44], and binding of substrates to enzymes [45,46] by using an appropriate surface coating. The displacements observed in these experiments (10 s of nm) are well above the detection limit of our method (1 nm) and occur over relatively slow timescales (10 s of min). The can-

Author's personal copy

tilever position is usually measured continuously, but the initial and final displacement values are sufficient to indicate a binding event. Therefore, our interferometric method can be used to perform cantilever-based biochemical detection experiments in array format.

When discussing the potential for cantilever arrays, it is instructive to consider the fluorescent DNA microarray [47], which is the workhorse of modern molecular biology. This device is based on a simple, disposable chip with thousands of sites and an external scanner that sequentially images all the sites. One scan is sufficient to detect the binding events at each site. Hence, the scan time is not critical and the array can be made very large, leading to massively parallel experiments. Our interferometric readout method can be used to measure cantilever arrays in a similar manner. Although the fluorescent microarray is an extremely successful technology, it has one major flaw: the target molecules must be fluorescently labeled. This complicates sample preparation. Moreover, in the case of protein microarrays, the label can modify the properties of the target protein and reduce detection specificity [48]. Cantilever arrays would overcome that problem since they do not require labeling.

The maximum number of measured cantilevers reported here is 8. Each device takes less than 1 min of measurement time, including taking initial and final images and processing them. Although this is a modest demonstration, there is considerable room for improvement. The image acquisition can be made much faster by using a microscope with a motorized stage and automatic focus adjustment. It can also be accelerated by placing the cantilevers close to each other on the chip so that multiple devices fit in the same image. Moreover, the need for taking initial images of each device would be eliminated if the cantilevers are made more similar to each other by improved fabrication process control. The image processing algorithm can also be automated further to reduce the amount of user input required by adding alignment marks on the device.

The measurement resolution of our method can be improved further, although, as discussed previously, it is already sufficient for typical biochemical detection experiments. More uniform microscope illumination and automatic focus adjustment would reduce the variability due to sample repositioning and refocusing. Higher optical magnification and higher resolution cameras would reduce the quantization error. Alternatively, more advanced image processing algorithms can be employed to detect sub-pixel fringe shifts [49].

6. Conclusion

This paper presents a new microcantilever sensor design and a method for measuring its displacement by tracking the interference fringes in its microscope image. We believe that this method is feasible for high-throughput readout of cantilever arrays. Unlike the conventional PSD-based readout approach, the alignment tolerance of the reader to the device is greatly relaxed, and the reader can be moved between devices after the sample is introduced. This allows the results of multiple parallel cantilever experiments to be captured by a single reader. In contrast with the cantilevers using integrated displacement sensors, our device is much simpler to fabricate and does not require external electrical connections. Moreover, our method is less prone to signal drifts and calibration errors than both the integrated senor and PSD approaches due to the interferometric nature of the measurements. The demonstrated readout speed is still modest, but it can be greatly improved by further automation of the image acquisition and analysis. We hope that this work is a step toward the realization of large label-free microcantilever arrays that can supplement the existing fluorescent microarray technology.

Acknowledgments

This work was funded by the Laboratory for Physical Sciences, the R.W. Deutsch Foundation, and the National Science Foundation (EFRI). We appreciate the support of the Maryland NanoCenter and its FabLab. We would also like to thank our collaborators in the Deutsch Project Group and colleagues at the MEMS Sensors and Actuators Lab at the University of Maryland.

Appendix A. Supplementary data

Supplementary data associated with this article can be found, in the online version, at doi:10.1016/j.snb.2010.02.038.

References

[1] N.V. Lavrik, M.J. Sepniak, P.G. Datskos, Cantilever transducers as a platform for chemical and biological sensors, Rev. Sci. Instrum. 75 (2004) 2229–2253.
[2] H.P. Lang, M. Hegner, E. Meyer, C. Gerber, Nanomechanics from atomic resolution to molecular recognition based on atomic force microscopy technology, Nanotechnology 13 (2002) R29–R36.
[3] L.G. Carrascosa, M. Moreno, M. Alvarez, L.M. Lechuga, Nanomechanical biosensors: a new sensing tool, TrAC, Trends Anal. Chem. 25 (2006) 196–206.
[4] R. Raiteri, M. Grattarola, H.-J. Butt, P. Skladal, Micromechanical cantilever-based biosensors, Sens. Actuators B 79 (2001) 115–126.
[5] J. Fritz, M.K. Baller, H.P. Lang, H. Rothuizen, P. Vettiger, E. Meyer, H.-J. Guntherodt, C. Gerber, J.K. Gimzewski, Translating biomolecular recognition into nanomechanics, Science 288 (2000) 316–318.
[6] M. Alvarez, L.G. Carrascosa, M. Moreno, A. Calle, A. Zaballos, L.M. Lechuga, C. Martinez-A, J. Tamayo, Nanomechanics of the formation of DNA self-assembled monolayers and hybridization on microcantilevers, Langmuir 20 (2004) 9663–9668.
[7] M. Su, S. Li, V.P. Dravid, Microcantilever resonance-based DNA detection with nanoparticle probes, Appl. Phys. Lett. 82 (2003).
[8] B. Illic, D. Czaplewski, H.G. Craighead, P. Neuzil, C. Campagnolo, C. Batt, Mechanical resonant immunospecific biological detector, Appl. Phys. Lett. 77 (2000).
[9] M. Calleja, J. Tamayo, A. Johansson, P. Rasmussen, L. Lechuga, A. Boisen, Polymeric cantilever arrays for biosensing applications, Sens. Lett. 1 (2003) 1–5.
[10] T. Braun, V. Barwich, M.K. Ghatkesar, A.H. Bredekamp, C. Gerber, M. Hegner, H.P. Lang, Micromechanical mass sensors for biomolecular detection in a physiological environment, Phys. Rev. E 72 (2005).
[11] X.R. Zhang, X. Xu, Development of a biosensor based on laser-fabricated polymer microcantilevers, Appl. Phys. Lett. 85 (2004) 2423–2425.
[12] H.P. Lang, M.K. Baller, R. Berger, C. Gerber, J.K. Gimzewski, F.M. Battiston, P. Fornaro, J.P. Ramseyer, E. Meyer, H.J. Guntherodt, An artificial nose based on a micromechanical cantilever array, Anal. Chim. Acta 393 (1999) 59–65.
[13] H.P. Lang, R. Berger, F. Battiston, J.-P. Ramseyer, E. Meyer, C. Andreoli, J. Brugger, P. Vettiger, M. Despont, T. Mezzacasa, L. Scandella, H.-J. Güntherodt, C. Gerber, J.K. Gimzewski, A chemical sensor based on a micromechanical cantilever array for the identification of gases and vapors, Appl. Phys. A 66 (1998) S61–S64.
[14] R. McKendry, J. Zhang, Y. Arntz, T. Strunz, M. Hegner, H.P. Lang, M.K. Baller, U. Certa, E. Meyer, H.-J. Guntherodt, C. Gerber, Multiple label-free biodetection and quantitative DNA-binding assays on a nanomechanical cantilever array, Proc. Natl. Acad. Sci. U.S.A. 99 (2002).
[15] P.A. Rasmussen, J. Thaysen, O. Hansen, S.C. Eriksen, A. Boisen, Optimised cantilever biosensor with piezoresistive read-out, Ultramicroscopy 97 (2003) 371–376.
[16] A. Johansson, M. Calleja, P.A. Rasmussen, A. Boisen, SU-8 cantilever sensor system with integrated readout, Sens. Actuators A 123–124 (2005) 111–115.
[17] B. Rogers, L. Manning, M. Jones, T. Sulchek, K. Murray, B. Beneschott, J.D. Adams, Mercury vapor detection with a self-sensing, resonating piezoelectric cantilever, Rev. Sci. Instrum. 74 (2003) 4899–4901.
[18] Y Lee, G. Lim, W. Moon, A self-excited micro cantilever biosensor actuated by PZT using the mass micro balancing technique, Sens. Actuators A 130–131 (2006) 105–110.
[19] D.R. Baselt, B. Fruhberger, E. Klaassen, S. Cemalovic, C.L. Britton, S.V. Patel, T.E. Mlsna, D. McCorkle, B. Warmack, Design and performance of a microcantilever-based hydrogen sensor, Sens. Actuators B 88 (2003) 120–131.
[20] J. Arcamone, G. Rius, G. Abadal, J. Teva, N. Barniol, F. Perez-Murano, Micro/nanomechanical resonators for distributed mass sensing with capacitive detection, Microelectron. Eng. 83 (2006) 1216–1220.
[21] G. Shekhawat, S.-H. Tark, V.P. Dravid, MOSFET-embedded microcantilevers for measuring deflection in biomolecular sensors, Science 311 (2006) 1592–1595.
[22] M. Nordström, D.A. Zauner, M. Calleja, J. Hübner, A. Boisen, Integrated optical readout for miniaturization of cantilever-based sensor system, Appl. Phys. Lett. 91 (2007) 103512.
[23] M.W. Pruessner, N. Siwak, K. Amarnath, S. Kanakaraju, W.-H. Chuang, R. Ghodssi, End-coupled optical waveguide MEMS devices in the indium phosphide material system, J. Micromech. Microeng. 16 (2006) 832–842.
[24] K. Zinoviev, C. Dominguez, J.A. Plaza, V.J.C. Busto, L.M. Lechuga, A novel optical waveguide microcantilever sensor for the detection of nanomechanical forces, J. Lightwave Technol. 24 (2006) 2132–2138.

Author's personal copy

[25] M. Helm, J.J. Servant, F. Saurenbach, R. Berger, Read-out of micromechanical cantilever sensors by phase shifting interferometry, Appl. Phys. Lett. 87 (2005) 064101.
[26] S.T. Koev, M.A. Powers, H. Yi, L.-Q. Wu, W.E. Bentley, G.W. Rubloff, G.F. Payne, R. Ghodssi, Mechano-transduction of DNA hybridization and dopamine oxidation through electrodeposited chitosan network, Lab Chip 7 (2007) 103–111.
[27] S.T. Koev, R. Ghodssi, Advanced interferometric profile measurements through refractive media, Rev. Sci. Instrum. 79 (2008) 093702.
[28] S.D. Senturia, Microsystem Design, Kluwer Academic Publishers, Boston, 2001.
[29] L.G. Brown, A survey of image registration techniques, ACM Comput. Surveys 24 (1992) 325–376.
[30] S.T. Koev, R. Fernandes, W.E. Bentley, R. Ghodssi, A cantilever sensor with an integrated optical readout for detection of enzymatically produced homocysteine, IEEE Trans. Biomed. Circ. Syst. 3 (2009) 415–423.
[31] D. Sameoto, S.-H. Tsang, I.G. Foulds, S.-W. Lee, M. Parameswaran, Control of the out-of-plane curvature in SU-8 compliant microstructures by exposure dose and baking times, J. Micromech. Microeng. 17 (2007) 1093–1098.
[32] G.C. Hill, R. Melamud, F.E. Declercq, A.A. Davenport, I.H. Chan, P.G. Hartwell, B.L. Pruitt, SU-8 MEMS Fabry–Perot pressure sensor, Sens. Actuators A 138 (2007) 52–62.
[33] J. Hossenlopp, L. Jiang, R. Cernosek, F. Josse, Characterization of epoxy resin (SU-8) film using thickness-shear mode (TSM) resonator under various conditions, J. Polym. Sci.: Part B: Polym. Phys. 42 (2004) 2373–2384.
[34] A.L. Olsen, E.R. Washburn, An interpolation table for refractive index–normality relationship for solutions of hydrochloric acid and sodium hydroxide, Trans. Kansas Acad. Sci. 40 (1937) 117–126.
[35] D.R. Lide, CRC Handbook of Chemistry and Physics, 85th ed., CRC Press, Boca Raton, FL, 2006.
[36] F. Schreiber, Self-assembled monolayers: from 'simple' model systems to biofunctionalized interfaces, J. Phys.: Condens. Matter 16 (2004) R881–R900.
[37] R. Berger, E. Delamarche, H.P. Lang, C. Gerber, J.K. Gimzewski, E. Meyer, H.-J. Güntherodt, Surface stress in the self-assembly of alkanethiols on gold probed by a force microscopy technique, Appl. Phys. A 66 (1998) S55–S59.
[38] R.F. DeBono, G.D. Loucks, D.D. Manna, U.J. Krull, Self-assembly of short and long-chain n-alkyl thiols onto gold surfaces: a real-time study using surface plasmon resonance techniques, Can. J. Chem. 74 (1996) 677–688.
[39] Y. Zhang, Q. Ren, Y.-P. Zhao, Modelling analysis of surface stress on a rectangular cantilever beam, J. Phys. D: Appl. Phys. 37 (2004) 2140–2145.
[40] M. Hopcroft, T. Kramer, G. Kim, K. Takashima, Y. Higo, D. Moore, J. Brugger, Micromechanical testing of SU-8 cantilevers, Fatigue Fract. Eng. Mater. Struct. 28 (2005) 735–742.
[41] D. Bachmann, B. Schoberle, S. Kuhne, Y. Leiner, C. Hierold, Fabrication and characterization of folded SU-8 suspensions for MEMS applications, Sens. Actuators A 130–131 (2006) 379–386.
[42] R. Feng, R.J. Farris, Influence of processing conditions on the thermal and mechanical properties of SU8 negative photoresist coatings, J. Micromech. Microeng. 13 (2003) 80–88.
[43] C. Grogan, R. Raiteri, G.M. O'Connor, T.J. Glynn, V. Cunningham, M. Kane, M. Charlton, D. Leech, Characterisation of an antibody coated microcantilever as a potential immuno-based biosensor, Biosens. Bioelectron. 17 (2002) 201–207.
[44] Y. Arntz, J.D. Seelig, H.P. Lang, J. Zhang, P. Hunziker, J.P. Ramseyer, E. Meyer, M. Hegner, C. Gerber, Label-free protein assay based on a nanomechanical cantilever array, Nanotechnology 14 (2003) 86–90.
[45] A. Subramanian, P.I. Oden, S.J. Kennel, K.B. Jacobson, R.J. Warmack, T. Thundat, M.J. Doktycza, Glucose biosensing using an enzyme-coated microcantilever, Appl. Phys. Lett. 81 (2002) 385–387.
[46] X. Yan, H.-F. Ji, Y. Lvov, Modification of microcantilevers using layer-by-layer nanoassembly film for glucose measurement, Chem. Phys. Lett. 396 (2004) 34–37.
[47] T. Joos, P. Fortina, Microarrays in Clinical Diagnostics, Humana Press, Totowa, NJ, 2005.
[48] P. Mitchell, A perspective on protein microarrays, Nat. Biotechnol. 20 (2002) 225–229.
[49] K. Takita, T. Aoki, Y. Sasaki, T. Higuchi, K. Kobayashi, High-accuracy subpixel image registration based on phase-only correlation, IEICE Trans. Fundam. E86-A (2003).

Biographies

Stephan Koev was born in Bulgaria in 1981. He received a BS degree in Electrical Engineering from the US Naval Academy in 2004, and MS and PhD degrees in Electrical Engineering from the University of Maryland in 2007 and 2009, respectively. His doctoral research was in the area of MEMS for biomedical applications. His interests include micro- and nano-fabrication, integrated optics, bio-device interfaces, and MEMS metrology. Currently, he is a postdoctoral research associate with the Center for Nanoscale Science and Technology at the National Institute of Standards and Technology, Gaithersburg, MD, USA.

William E. Bentley is the Robert E. Fischell Distinguished Professor and Chair of the Fischell Department of Bioengineering at the University of Maryland. He holds joint appointments with the Maryland Technology Enterprise Institute (MTECH) and the University of Maryland Biotechnology Institute. He received his B.S. and M.S. from Cornell University and his Ph.D. from the University of Colorado, Boulder, all in chemical engineering. His research interests include biomolecular and metabolic engineering, cell-to-cell communication, heterologous protein expression, and device/bio interfaces. Dr. Bentley is a fellow of the American Institute of Medical and Biological Engineers, the American Association for the Advancement of Science and the American Academy of Microbiology.

Reza Ghodssi is the *Herbert Rabin Distinguished Professor* and Director of the MEMS Sensors and Actuators Lab (MSAL) in the Department of Electrical and Computer Engineering (ECE) and the Institute for Systems Research (ISR) at the University of Maryland (UMD). Dr. Ghodssi's research interests are in the design and development of microfabrication technologies and their applications to micro/nano-devices and systems for chemical and biological sensing, small-scale energy conversion and harvesting. Dr. Ghodssi has over 70 scholarly publications, is the co-editor of the "Handbook of MEMS Materials and Processes" to be published in 2009, and is an associate editor for the Journal of Micorelectromechanical Systems (JMEMS) and Biomedical Microdevices (BMMD).